POLITECNICO DI MILANO

Faculty of Information Engineering
Master of Science in Telecommunications Engineering
Electronics, Information and Bioengineering Department

POLITECNICO
MILANO 1863

28 GHZ APPLICATIONS, PATH LOSS MODELS AND COVERAGE FOR 5G

Advisor: Prof. Michele D'AMICO

Candidate:
MEI FEIYING   ID: 893731

Academic Year 2018–2019

Abstract

Recent advances in the 5G wireless technologies are demanding higher bandwidth. In this thesis, there are some applications for 5G focusing on mmWave frequency band at 28 GHz and many companies and research groups have proposed measurements and models. The 28 GHz omnidirectional path loss models are compared for urban environments, especially the outdoor scenario. And the models are also compared in the physical environment which is classified as line of sight (LOS) or non-line of sight (NLOS) between the transmitter (TX) and the receiver (RX). In addition, according to analysis of LOS probability, the simulation of a base station coverage at 28 GHz for an elevation area of 1000x1000 m2 is proposed, which indicates that the distance between the TX and RX ranges from10 m to 100 m, the probability of LOS is higher than the value of 20%.

List of Abbreviations

5G	Fifth Generation
LTE	Long Term Evolution
LOS	Line of Sight
NLOS	Non Line of Sight
TX	Transmitter
RX	Receiver
UMa	Urban Macro
O2I	Outdoor-to-Indoor
LMDS	Local Multipoint Distribution Service
CR	Continuous-Route
DOA	Direction-of-Arrival
AOA	Angle-of-Arrival
PLE	Path-Loss Exponent
PDP	Power Delay Profile
MMSE	Minimum Mean Square Error
SSCM	Statistical Spatial Channel Model
RF	Radio frequency
UMi	Urban Micro
CI	Close-In
ABG	Alpha-Beta-Gamma
CIF	CI model with a Frequency-weighted
V-V	Vertical-to-Vertica

V-H	Vertical-to-Horizontal
KED	Knife-Edge Diffraction
mmWave	Millimeter Wave
3GPP TR 38.901,	The 3rd Generation Partnership Project
5GCM	5G Channel Model
METIS	Mobile and wireless communications Enablers for the Twenty–twenty Information Society
MmMAGIC	Millimeter-Wave Based Mobile Radio Access Network for 5G Integrated Communications
BPL	Building Penetration Loss
MT	Mobile Terminal
SNR	Signal-to-Noise Ratio
BW	BandWidth
NF	Noise Figure
BS	Base Station
MDS	Minimum Detectable Signal
IAB	Integrated Access Backhaul
UE	User Equipment
NR	New Radio
gNB	Next Generation NodeB
DL	DownLink
UL	UpLink

Contents

List of Figures

List of Tables

Chapter 1

1.1 Introduction

Due to the continuous use of video and the increase in the Internet of Things, the growing demand for faster data rates and more bandwidth is driving research into next-generation cellular communication systems. While using lower frequency bands to minimize cost and provide simplicity, it is not enough to support higher data rates, as required by next-generation communication standards. The use of higher frequency bands, especially millimeter waves in the system, means smaller coverage areas, but may provide smaller antennas and enough data rates for each mobile station, far greater than currently available [1]. The arrival of 5G will provide multiple simultaneous connections for more than one hundred to several thousand devices, indoor users can achieve higher data rates of up to 1 Gbps, and for all devices connected to the Network [2], the minimum end-to-end delay can be as low as 1 ms. The millimeter wave bands promise a large amount of unlicensed spectrum at 28 GHz and 39 GHz and is a potential band for 5G cellular systems. In order to optimally design a millimeter wave wireless system, the main requirement is to understand the radio channel in terms of frequency and use-cases of interest.

Over the past few years, many companies and research groups have proposed measurements and models for the 28 GHz band, with a focus on indoor or urban scenarios [5]–[22]. The 5G mmWave wireless

channel bandwidth will be more than ten times higher than today's 4G Long Term Evolution (LTE) 20 MHz cellular channel. In order to generate reliable models for future millimeter-wave system designs, path loss models must be established for link budget and signal strength prediction, including directional and beamforming antenna arrays.

In the 28 GHz millimeter wave band, atmospheric absorption does not significantly increase the extra path loss, making it suitable for outdoor mobile communications. In order to study urban cellular propagation, it is customary to classify the physical environment as line of sight (LOS) or non-line of sight (NLOS) between the transmitter (TX) and the receiver (RX). NLOS can be further divided into moderately and severely obstructed environments, where medium NLOS conditions have small obstacles, such as trees or building edges that partially block the optical path between TX and RX, while severely blocked NLOS conditions have large obstructions fully blocking the optical path.

1.2 Thesis outline

The structure of this paper is as follows. Chapter 2 introduces the main theoretical foundations of the propagation phenomenon, including the mechanisms of communication, the effects on propagation and fading. Then, some applications of 5G at 28 GHz and 39GHz are summarized.

Chapter 3 focuses on the 28 GHz omnidirectional path loss model for urban environments, including outdoor, indoor, and O2I (penetration loss), and then compares different models.

Chapter 4 begins with a description of the base stations that cover the coverage area, link budget, and related products. Next, the analysis of the mobile terminal is introduced, and then the application of the integrated access backhaul in the millimeter wave network is proposed.

Chapter 5 focuses on probabilities of line-of-sight and non-line-of-sight, and then presents simulation results for a base station coverage in a 28 GHz UMa scenario.

Chapter 6 gives the conclusions.

Chapter 2

Propagation Basics

In order to understand the basis of propagation, it is important to describe how the communication between the transmitter and the receiver occurs and the propagation mechanism that occurs. A statistical description of the propagation channel is provided along with a specific classification of the phenomena encountered each time the radio wave propagates along the channel. Since measurements can be taken when propagation occurs, accurate statistical characterization of the channels can be performed, and useful general models can be created. Furthermore, since the communication between the transmitter and the receiver in a wireless environment is highly dependent on the propagation channel, it is important to give an accurate description and characterization of possible propagation phenomena and mechanisms.

2.1   Propagation Phenomena

Various phenomena may be encountered during the propagation of radio waves along the communication channel. In the following subsections, accurate and detailed classification and description are given for the most important cases: reflection, diffraction, scattering, shadowing and multipath fading [16].

2.1.1 Propagation Mechanisms

The ideal propagation between two points in visibility conditions is called direct propagation.

When the wave propagating from the transmitter to the receiver encounters obstacles with large size w.r.t. wavelength, it generates reflection (see Figure 2.1). In fact, part of the wave is transmitted to the receiver and the other part is reflected to the same medium. The characteristic guiding this phenomenon is the fact that, denoting with ϑI the angle of incidence and ϑR the angle of reflection, which are equal:

$$\vartheta_I = \vartheta_R \tag{2.1}$$
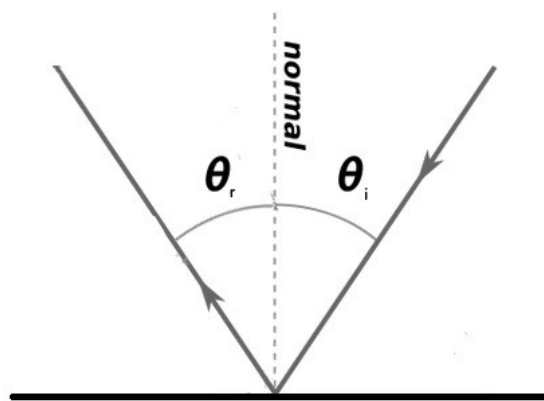
Figure 2.1: The reflection law
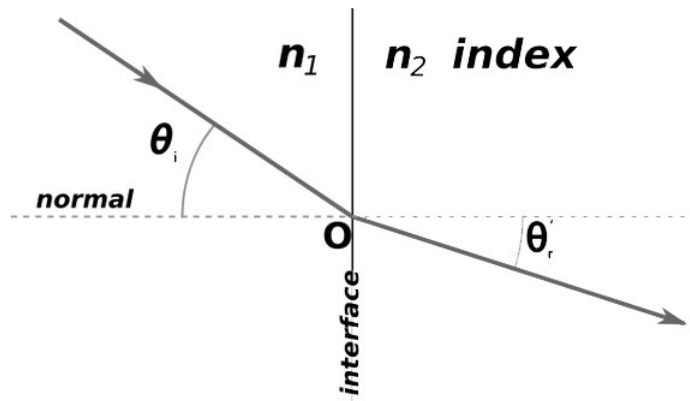
Figure 2.2：The Snell's law

Refraction, which occurs when waves propagate on layers with different refractive index (i.e different materials with different refractive index $n_2 < n_1$) and change its velocity. It is regulated by the Snell's law (see Figure 2.2) [3]:

$$n_1 \sin(\vartheta_1) = n_2 \sin(\vartheta_2) \qquad (2.2)$$

Another possible phenomenon that a radio wave can encounter when propagating along a propagation scenario is diffraction. It happens when the path is obstructed by an obstacle with sharp edge (like the edge of a building such as rooftops or the edge of a hill). This phenomenon can be explained by the Huygens principle, which states that the wave front can be seen as a superposition of many fundamental isotropic sources.

2.1.2 Effects on Propagation

The main physical phenomena that have a negative impact on propagation are

- Multiple scattering mainly produced by rain at frequencies with wavelengths comparable to drops size. The impact is a potentially strong attenuation at frequencies above 10 GHz;

- Absorption due to molecular interactions between e.m. waves and atmospheric gases such as oxygen and water vapor. Sometimes, as the wave passes through a dark or opaque

medium, part of the signal strength is lost (i.e. the signal is neither reflected nor refracted).

- Thermal, atmospheric noise received by the antenna, atmospheric electrical phenomena (e.g. lightning).

Three channel components make up the entire channel model Wireless system [3]:

1. Path loss, the large-scale deterministic relationship between the link distance d and the average attenuation in a given environment (Sect. 2.1.3).

2. Shadow, i.e. large-scale ("slow"), due to the presence of large obstacles (buildings, hills...) resulting in random attenuation fluctuations in path loss that completely or partially obscure the propagation path. The change in path loss is a Gaussian distribution random variable with a standard deviation σ_{SH} in dB domain (between 2 and 8 dB in typical urban and suburban environments), which represents the shadow effect in the path loss. Statistical models are often used to characterize random attenuation; in the case of shadows, log-normal distributions are used [16]:

$$f_A(A_{SH}) = \frac{1}{\sqrt{2\pi}\sigma_{SH}}\exp(-\frac{(A_{SH}-\mu)^2}{2\sigma_{SH}^2}) \tag{2.3}$$

The variable A_{SH} is the additional attenuation in dB w.r.t. the path loss, μ is the mean typically equal to 0.

3. Due to multiple reflections at the receiver, multipath fading, ie small scale ("fast"), random attenuation fluctuations around large-scale attenuation (path loss + shadow). The multipath fading model also allows for the definition of channel impulse response (Sect. 2.2.1).

2.1.3 Free Space Path Loss: The Simplest Propagation Model

The ideal propagation situation is that electromagnetic waves

propagate in free space, i.e. in the absence of obstacles, such as walls, terrain, buildings and other objects in line of sight conditions (LOS). Since the environment is ideal and empty, the only form of attenuation here is the attenuation due to the distance; the greater the distance, the higher the attenuation experienced by the wave (i.e. the wave attenuation as the distance increases). The Friis' formula describes the free-space path loss between the transmitter and receiver.

EIRP is defined as the equivalent isotropic radiated power of a transmitter that radiates power Pt through an antenna transmitting gain Gt; alternatively, it can be defined as the power produced by an isotropic antenna with a peak power density in the direction of maximum gain. It is defined as [3]:

$$EIRP = P_t G_t \tag{2.4}$$

At receiver side, the effective area A_e is defined as the area that is available at the receiver to capture the signal coming from the transmitter oriented perpendicular to the direction of the coming radio wave. It is a function of the gain of the receiver antenna G_r, the wavelength λ of the transmitted signal and is defined as follows:

$$A_e = \frac{\lambda^2}{4\pi} G_r \tag{2.5}$$

After defining both the EIRP and the effective area Ae, it is possible to get the Friis' relation, defining the received power Pr at distance d from the transmitter as:

$$P_r = EIRP \times Ae = P_t G_t G_r \left(\frac{\lambda}{4\pi d}\right)^2 \tag{2.6}$$

Finally, the received signal power falls off inversely proportional to the square of the distance between the transmit and receive antennas and the free space attenuation [16] is given by

$$PL = \left(\frac{4\pi d}{\lambda}\right)^2 \tag{2.7}$$

2.2   Fading

In wireless communication, fading represents a random attenuation in path loss that varies due to various propagation phenomena such as reflection, refraction, diffraction or scattering; this is what is called large scale fading. However, there are many other important phenomena that need to be described and analyzed that have a large impact on the received signal; they can be combined as small scale fading effects.

2.2.1 Multipath Fading

The first effect is due to the presence of multipath fading. Multipath attenuation results from a combination of more signal components (ie, reflection, diffraction, scattering, and shadow) at the receiver, with phase and amplitude differences, direction and field strength (Figure 2.3). The LOS components will have higher energy because they will not encounter any obstacles in the path but will encounter the NLOS components with lower signal strength and greater travel distance. The total field will be the combinations of LOS and NLOS components that can be destructively constructive depending on the phase value; therefore, the total field can be increased or decreased depending on these factors [3].
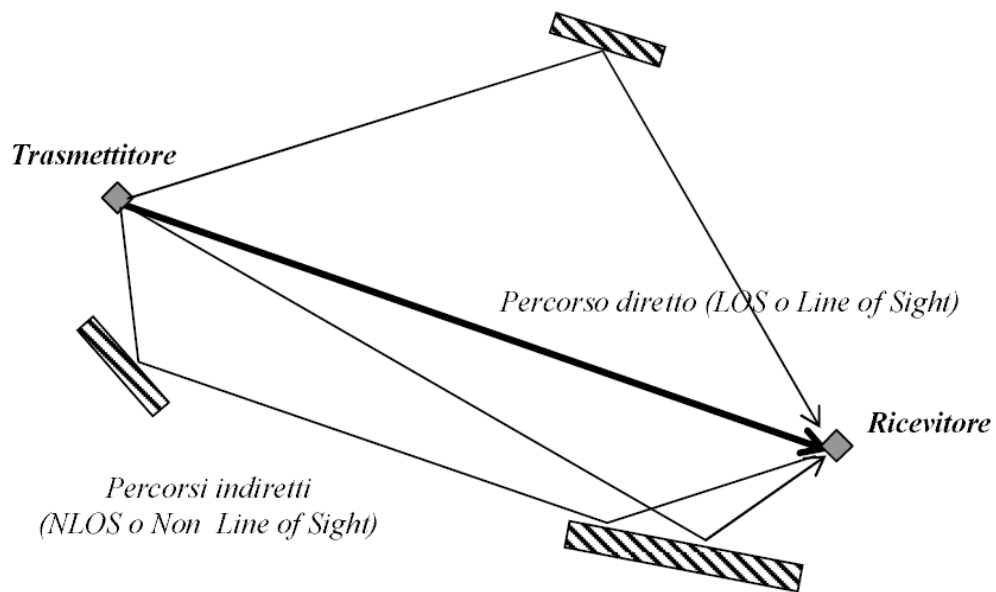
Figure 2.3: The multipath fading

In presence of dense multipath, according to the Central limit theorem, the sum of multiple contributions can be considered as a complex valued random variable with a normal (Gaussian) distribution. Under Gaussian assumption, there are two propagation conditions: (i) the absence of dominant or fixed components (typical non-line-of-sight condition) and (ii) the presence of dominant or fixed components (typically the presence of direct waves line-of-sight condition). In former case the channel is a Rayleigh fading channel and in the latter case the channel is a Ricean fading channel.

2.2.1.1 Rayleigh Distribution

It is used to characterize small-scale fading of signals in case of an infinite number of adjacent paths, without the presence of a dominant component and casual phases value, uniform in the range $[0,2\pi]$. The probability density function of the Rayleigh distribution of a random variable α defined for $\alpha \geq 0$, can be expressed as [3] [4]:

$$f_\alpha(\alpha) = \frac{\alpha}{\sigma^2} \cdot \exp(-\frac{\alpha^2}{2\sigma^2}) \tag{2.8}$$

Then mean value $E[\alpha] = \sigma\sqrt{\pi/2}$.

2.2.1.2 Rician Distribution

It is used when the Rayleigh assumptions are not verified since there is a LOS component with a higher signal strength compared to the other paths and many other reflected paths. The probability density function can be expressed as a casual Rice variable α defined for $\alpha \geq 0$ [3] [4]:

$$f_\alpha(\alpha) = \frac{\alpha}{\sigma^2} \cdot \exp(-\frac{\alpha^2 + b^2}{2\sigma^2}) \cdot I_0(\frac{b\alpha}{\sigma^2}) \tag{2.9}$$

where $I_0(\alpha)$ is the modified Bessel function of the first kind with order zero. The phase θ can be considered, again, uniformly distributed in $[0, 2\pi]$. Moreover, it is important to describe how the direct component is dominating on the others and the ratio between the direct and diffused components is called Rice factor $K = b^2/2\sigma^2$, the closer K is to 0, the Rice gets closer to the Rayleigh one)

2.2.2 Doppler Effects

Another important effect of big interest is called doppler effect. It is characterized and defined using different parameters: Doppler spread and coherence time, delay spread and coherence bandwidth.

The received signal turns out to be a sinusoid shifted by a frequency offset:

$$f_D = f_c \frac{v}{c} \qquad (2.10)$$

When the propagation direction is not parallel to the velocity v but forms an angle ϑ, it is enough to consider the component of relative motion at a certain velocity v with respect to the transmitter and the Doppler shift is expressed as [4]:

$$f_D = f_C \cdot \frac{v}{c} \cdot \cos\vartheta = \frac{v}{\lambda} \cdot \cos\vartheta \qquad (2.11)$$

Moreover, the coherence time T_c is used to give a better description of the time interval where the channel remains approximately constant and quasi-static. It is proportional to the inverse of the maximum frequency dispersion (Doppler dispersion) denoting as $\Delta f_D = 2f_{D,MAX}$; it means that in that time interval the channel characteristics are not significantly changing. It can be expressed as

$$T_C = \frac{k}{\Delta f_D} \qquad (2.12)$$

with typical values of k equal to 1/5 or 1/10.

Denoting by τ_{max} the maximum delay w.r.t. the first path in a wireless channel, the non distortion condition will be given by $B_W \ll 1/\tau_{max}$.

It is useful to define also the coherence bandwidth that states which is the bandwidth within which the signal can be considered not distorted from the channel. It can be expressed as [3]:

$$B_C = \frac{k}{\tau_{max}}$$

2.3   Conclusions of applications for 5G at 28 GHz

In the past few decades, in order to gain a deep understanding of the spatial and temporal characteristics of the mmWave band, various measurement activities have been carried out in order to develop new techniques and methods to operate it. The following sections describe the various applications in the 28 GHz band focusing on indoor or urban.

Work in [5] presented the results of a wide range of on-site measurement procedures conducted by Hewlett Packard in a suburban environment to characterize 28 GHz radio wave propagation for local multipoint distribution services. The LMDS coverage varied with cell size, location and height of the hub antenna, and the nature of the service area (urban and suburban). 80% coverage was achieved on the suburban area of San Jose using an 80 ft. hub antenna and a 2 km cell radius. An advanced LMDS planning tool has been developed to accurately assess and maximize the relationship between coverage and hub antenna height and position.

In [6] the authors described a model for building corner diffraction losses at 28 GHz based on a series of propagation measurements, which reported here were made at three separate buildings, and each building has a sharp 90° corner that was near the middle of the path. The diffraction angle was the key variable in the characterization of diffraction losses, and diffraction losses showed little dependence on building material, polarization, and path length. And then a mathematical model to characterize the diffraction losses was developed, which was piecewise for the two regions "small angle diffraction" and "large angle diffraction". The model showed agreement with the theory and data points measured.

In [7] Local Multipoint Distribution Service (LMDS) is a cellular system that has become a two-way broadband technology. The behavior of a typical LMDS system was simulated using a wide beam antenna for the transmitter and a more directional antenna for the receiver. This work was to parameterize the urban areas namely as a function of the statistical heights and width distributions and then used the system to measure the different locations of Madrid's four parameterized environments. The results obtained can accurately characterize the different environments used for LMDS.

The paper [8] presented and analyzed the results of millimeter-wave 60-GHz frequency range propagation channel measurements performed in various indoor environments for CR and DOA measurement activities. The statistical parameters of the propagation channel, such as the number of paths, RMS delay spread, path loss and shadowing, and the interdependencies of different characteristics of the multipath channel had been investigated. A linear relationship between the number of paths and delay spread can be established, and a negative cross-correlation between shadow fading and delay spread had been found. Based on DOA measurements that were performed in rooms and corridors in LOS and NLOS scenarios. It had been found that it is sufficient to consider direct waves and first-order reflected waves from smooth surfaces in the case of LOS, and diffraction was an important propagation mechanism in the NLOS propagation environment. Empirical modeling results can be used to design 60 GHz radio systems for short-range wireless applications.

Measurements at 28 GHz and 38 GHz were performed in urban microcellular environments in New York City and Austin, Texas, respectively [9]. The measurements were performed using state-of-the-art sliding correlator channel detectors, and antennas of various heights and gains were available in a variety of combinations of steerable

transmit and receive in both line-of-sight and non-line-of-sight situations. Based on the measured data, a new large-scale path loss model of millimeter wave propagation channel in urban microcellular environment was given by using the floating intercept. The shadow fading effect in urban microcellular environments was proposed and simulated. Specifically, the model showed that New York City's shadow factor was reduced by about 1 dB, and the shadow factor in Austin, Texas was reduced by about 6 dB. The model also showed that in future millimeter-wave communications, mobile devices should deploy antennas with higher gains to compensate for additional path loss due to frequency hopping from low microwave to millimeter wave states.

The world's first 28 GHz outdoor cellular propagation measurement for (5G) mobile communications was conducted in New York City [10], which used a 400 MPa/sec (Mbps) sliding correlator channel sounder and directional horn antennas. All three TX sites used the same set of 25 RX sites, thus producing 75 TX-RX location combinations. In all locations, both TX and RX use a 24.5 dBi antenna with a beamwidth of 10∘3dB. The overall PLE, LOS and NLOS for all measurements was 5.73. When only the best NLOS link was considered at each RX location, the PLE was reduced to 4.58. When performing a 10° incremental azimuth scan, the received PDPs were measured with less than 168 dB path loss at more than 22 of 36 possible azimuths in the urban NLOS environment. For the LOS and NLOS environments, PDPs of the observed maximum multipath delay spread are 753.5 ns and 1388.4 ns, respectively. In addition, 57% of the TX-RX intervals of the receiver position exceeding 200 meters were outages, but within 200 meters, the outage was reduced to 16%.

In [11] Propagation measurement at 28 GHz was conducted around the downtown Brooklyn using 83 TX-RX locations. The TX and RX

antennas are mechanically controlled in 10° increments in azimuth using a 400 megabit per second channel depth sounder with vertically polarized 24.5 dBi horn antenna (3 dB beamwidth 10.9°). Small-scale measurements were performed in with a step length of 5.35 mm (λ/2) along a 107 mm (10λ) length orbit, demonstrating little fading with a $\pm$ 2 dB fluctuation about the mean power level at a given AOA, and that an average of 2.5 signal lobes from TX to RX were discovered. Using the MMSE method, the lobe path loss exponent is n = 5.52, which was found with respect to a 5 m free space reference lobe, and the shading factor is 10.9 dB. These models will be used to create a 28 GHz SSCM for future 5G cellular networks.

The measurement of the 38 GHz outdoor cellular channel was performed in an urban environment with a wideband sliding correlator channel sounder [12]. Extensive angles of arrival, path loss and multipath time delay spread measurements were performed for steerable beam antennas with different gain and beamwidth for various transmitter and receiver positions. The large environmental dependence of the receiver and emitter AOA distributions indicated the usefulness of site-specific cell design using ray tracing models. The likelihood of coverage interruption and steerable antenna interruptions was also measured to determine how random receiver locations with different antenna gains and link budgets would be performed in future cellular systems. Lower base stations were capable of using many reflectors in the environment to cover all locations within a 200-m radius from the base station. The measurements and models presented in this paper may be used to design future fifth-generation millimeter-wave cellular networks and gain insight into the antenna beam steering algorithms for these systems.

Work in [13] propagation measurements at 28 GHz of reflection coefficients and penetration losses were conducted in New York City,

utilizing a 400 megabit per second channel sounder and 24.5 dBi steerable horn vertically polarized antennas. Reflections from walls and buildings and penetration losses were measured for various materials, such as tinted glass, clear glass, brick, concrete, and drywall. The 28 GHz outdoor material had a larger reflection coefficient for the tinted glass compared to the less reflective indoor building materials, which was 0.896. It was clear that indoor-to-outdoor penetration was quite difficult, whereas the propagation was easily supported by the strong reflectivity of external building materials and low attenuation of indoor materials, and showed that high penetration loss through brick and tinted glass, as well as low attenuation through clear glass and drywall. Further, it was found that the values for penetration losses through indoor walls, were dependent on the TX-RX separation distance and the number of penetration obstructions, but also on the surrounding environment.

In [14] the authors introduced the newly generated omnidirectional close-in free space reference distance and floating-intercept path loss models at 28 GHz and 73 GHz obtained from ultrawideband 800 MHz RF null-to-null bandwidth measurements collected in Downtown Manhattan using a 400 Mcps broadband sliding correlator channel sounder. This provided a simplified path loss model for the 1 m close-in free-space reference distance for the omnidirectional propagation model and is suitable for system-level simulation and design, similar to the 3GPP and WINNER II. The 28 GHz and 73 GHz measurements showed that compared to the UHF/microwave channel, the mmWave channels were more directional on TX and RX. The prospect of beamforming and beam combining techniques for mobile handsets using electrically phased on-chip antenna arrays would require mmWave directional path loss models that allowed one to estimate the received power level in a narrow-given direction.

The paper [15] provided large-scale path loss data for 28 and 73 GHz urban omnidirectional propagation measured in downtown New York in the summers of 2012 and 2013, and 38 GHz data measured in downtown Austin in the summer of 2011. The data presented here can be used for antenna, propagation and communications researchers in emerging mobile and/or backhaul mmWave system analysis. Descriptions of the directional measurements for calculating omnidirectional large-scale path loss data were given, providing map-based layouts of 28 GHz and 73 GHz measurement activities for specific site modeling, and tabulated omnidirectional large-scale path loss data in LOS and NLOS environments at 28 GHz, 38 GHz, and 73 GHz were presented. Using the data provided herein, large-scale path loss models using a standard close-in 1 meter free-space reference distance were provided for each of the three frequency bands.

Work in [16] presented 28 GHz and 73 GHz indoor propagation directional and omnidirectional path loss models from two extensive UWB propagation measurement activities using 400 mega chip-per-second broadband sliding correlator channel detectors and highly directional steerable15 dBi and 20 dBi horn antennas. In LOS, the omnidirectional path loss exponents were 1.1 and 1.3 at 28 GHz and 73 GHz, and 2.7 and 3.2 in NLOS at 28 GHz and 73 GHz, respectively. When considering arbitrary unique pointing angles, the directional path loss exponents were measured at 4.5 and 5.1 at 28 GHz and 73 GHz, respectively, but were reduced to 3.0 and 4.3 when searching for the strongest TX-RX angle pointing link at each RX. The positioning RMS delay spread were 18.4 ns and 13.3 ns, respectively, with a maximum of 193 ns, 287.5 ns at 28 GHz and 73 GHz in LOS and NLOS environments. The channel model provided here can be used for mmWave system-wide simulations and radio system design in the indoor environment.

This paper described the mmWave propagation measurements in UMi Scenior and indoor office scenarios at 28 GHz and 73 GHz [17], and used the data from the measurement activities to present and compare single-frequency FI and CI path loss models, as well as multi-frequency ABG, CI and CIF models. The results showed that the CI and CIF models provided physical basis, simplicity and robustness over the frequencies and distances, when compared to the FI and ABG models. Furthermore, path loss in outdoor environments had little dependence on frequencies beyond the first meter of free space propagation, while path loss tended to increase with frequency in indoor environments. Therefore, compared to the ABG and CIF models, the CI model was best suited for outdoor mmWave environments, while the CIF model was superior to ABG and CI for indoor environments. The CI and CIF models used fewer parameters and provided more convenient closed-form expressions for analysis.

In this paper [18], the statistics of mmWave outdoor small-scale fading were obtained by 28 GHz measurements in the local area in LOS and NLOS environments using a wideband sliding correlator channel detector and a pair of high gain directional horn antennas. The voltage path gain amplitude display followed the Rician distribution with a K factor of 9-15 dB in the LOS, a 5-8 dB NLOS in the VV scenario, and a 3-7 dB VH scenario in the LOS and NLOS, respectively. Similarly, in the LOS to NLOS case, the K factor in the V-V scene is 4-6 dB, and in the V-H scene is 6-10 dB. Note that the average spatial autocorrelation function of each multipath component was calculated, indicating that the signal reaches zero correlation after 2 and 5 wavelengths in LOS and NLOS, respectively, for V-V antenna scenarios. When studying the multi-element diversity scheme of the next-generation millimeter-wave system, the model provided can be used to reconstruct the path gain statistics of the millimeter-wave wide-

19

band channel impulse response over the local area.

This paper [19] described the channel characteristics of the 28 and 73 GHz spectrum and compared the results with the currently used 2.14 GHz LTE-A band. The urban microcell LOS scene was then created using the ABG free space path loss propagation model. Network performance was investigated by estimating the average user throughput, average cell throughput, user throughput of cell edge users, peak user throughput, spectrum efficiency, and fairness index for different numbers of users in the cell. The results showed a significant 95% improvement in spectral efficiency at 28 GHz and 180% at 73 GHz compared to 2.14 GHz. In addition, the 28 and 73 GHz bands could deliver up to 80 and the average cell throughput was significantly increased by 170% compared to the current LTE-A band. These findings were useful for testing and implementing real environments and provided a vision for next generation 5G wireless communication networks.

In [20] the authors outlined the characteristics of the fifth generation (5G) wireless communication system currently being developed for the millimeter wave (mmWave) band and summarized the key 5G system concepts of the emerging mmWave wireless communication networks. 5G propagation challenges and antenna technologies were introduced and the channel modeling efforts of many international groups for both licensed and unlicensed applications were described here. Propagation parameters and channel models used to understand mmWave propagation, such as LOS probabilities, large-scale path losses, and building penetration losses, as developed by groups and standards bodies, were compared in the 0.5-100 GHz range. These organizations included 3GPP TR 38.901, 5GCM, METIS, mmMAGIC. The development of the correct propagation model is critical to the long-term development of future mmWave wireless systems and the basic

understanding of future engineers and students.

Propagation measurements investigated diffraction, human blocking effects, small-scale spatial fading and autocorrelation, local-area channel transitions, and signal power stability in local area clusters at mmWave frequencies [21]. The knife-edge diffraction (KED) and creep wave linear models were used to fit the diffraction loss results of 10 to 26 GHz and showed that the 73 GHz human blockage measurement was consistent with the double KED model. In most cases, under LOS and NLOS conditions, the small-scale fading of the mmWave received signal voltage amplitude is typically the omnidirectional and directional receive antenna pattern of the Ricean distribution. The small-scale autocorrelation of the received voltage amplitudes applied to the sinusoidal exponential and exponential functions of the LOS and NLOS environments, respectively, with a small decorrelation distance of 0.27-13.6 cm. Local area measurements using clustering and path scenes showed how the received signal changes as the mobile device moves from LOS and transitions to the NLOS position. The wideband mmWave power levels were faded from 0.4 dB per ms to 40 dB per s, depending on the speed of travel and the surroundings.

Work in [22] showed the millimeter wave propagation characteristics included free-space loss, atmospheric attenuation, rain-induced fading, foliage attenuation, material penetration and other propagation factors. Then, the survey showed the channel modeling efforts and the limitations of existing channel models were lack of measurements, 3D models, bandwidth, spatial characteristics, dual mobility, directional antennas, large-scale antennas. Furthermore, there were three models, including path loss model, narrowband channel model, wideband channel model. Finally, it showed an overview of both the steps towards generating the channel model and system design

considerations as well as associated antenna design guidelines such as antenna arrays, array gain and beamwidth. The link budget of the communication system is then analyzed, which depends on the base station' s and the mobile station' s, such as the transmit power, antenna gain, signal-to-noise ratio and the required throughput of the link.

Chapter 3

Comparison Among Different Models

3.1 Introduction

This chapter focuses on the 28 GHz omnidirectional path loss model for urban environments, including outdoor, indoor, and O2I (penetration loss). There are three basic types of large-scale path loss models to predict mmWave signal strength over distance for the vast mmWave frequency range. These include the close-in free space reference distance (CI) path loss model (with a 1 m reference distance) , the CI model with a frequency-weighted (CIF model) or height-weighted (CIH model) PLE, and the floating intercept (FI) path loss model, also known as the ABG model because of its use of three parameters α, β,and γ. A comparison of the different models is also presented below.

The path loss models introduced by the four major organizations, which include:

1) The 3rd Generation Partnership Project (3GPP TR 38.901), which attempts to provide channel models from 0.5–100 GHz based on a modification of 3GPP's Extensive effort to develop models from 6 to 100 GHz in TR 38.900.

2) 5G Channel Model (5GCM), an ad-hoc group of 15 companies

and universities that developed models Based on extensive measurement campaigns and helped Seed 3GPP understanding for TR 38.900.

3) Mobile and wireless communications Enablers for the Twenty–twenty Information Society (METIS), a Large research project sponsored by European Union.

4) Millimeter-Wave Based Mobile Radio Access Network For 5G Integrated Communications (mmMAGIC), another large research project sponsored by the European Union.

3.2 Outdoors: UMi-Street Canyon, UMi-Open Square and UMa

3.2.1 UMi-Street Canyon, UMi-Open Square Path loss

For UMi Large-Scale Path Loss, it is mainly measured in these two scenarios, including UMi-Street Canyon and UMi-Open Square. 5GCM [23] : Select the CI model to model the UMi LOS path loss, because the α in the ABG model is almost the same as the PLE of the CI model, and γ is very close to 2, which is the equation based on the physics-based Friis'free space prediction and used in the CI model. The CI and ABG models were used for UMi NLOS in 5GCM, and the parameter values for the CI and ABG models are given in Table 3.1. 3GPP TR 38.901: Path loss model using 3-D T-R separation distance d_{3D}, which considers BS height (h_{BS}) and UE height (h_{UE}). A mathematical patch for correcting model defects is used to set the lower limit of the NLOS model to the LOS path loss. METIS: The path loss model for UMi in METIS is a modified version of the ITU-R UMi path loss model, which is said to be valid for frequencies from 0.8 to 60 GHz. mmMAGIC: The mmMAGIC project uses UMi's ABG path loss model, like 5GCM but with different parameter values (see Table 3.1 and 3.2).

			PL [dB], f_c is in GHz and d_{3D} is in meters	Shadow fading std [dB]	Applicability range and Parameters
UMi-Street Canyon	5GCM	LOS	**CI model with 1 m reference distance:** $PL = 32.4 + 21\log_{10}(d_{3D}) + 20\log_{10}(f_c)$	$\sigma_{SF} = 3.76$	$f_c = 28GHz$
		NLOS	**CI model with 1m reference distance:** $PL = 32.4 + 31.7\log_{10}(d_{3D}) + 20\log_{10}(f_c)$ **ABG model:** $PL = 35.3\log_{10}(d_{3D}) + 22.4 + 21.3\log_{10}(f_c)$	$\sigma_{SF} = 8.09$ $\sigma_{SF} = 7.82$	$f_c = 28GHz$
	3GPP	LOS	$PL_{UMi-LOS} = \begin{cases} PL_1, & 10m \le d_{2D} \le d'_{BP} \\ PL_2, & d'_{BP} \le d_{2D} \le 5km \end{cases}$ $PL_1 = 32.4 + 21\log_{10}(d_{3D}) + 20\log_{10}(f_c)$ $PL_2 = 32.4 + 40\log_{10}(d_{3D}) + 20\log_{10}(f_c)$ $-9.5\log_{10}((d'_{BP})^2 + (h_{BS} - h_{UE})^2)$	$\sigma_{SF} = 4.0$	$f_c = 28GHz$ $1.5m < h_{UE} < 22.5m$ $h_{BS} = 10m$
		NLOS	$PL = \max(PL_{UMi-LOS}(d_{3D}), PL_{UMi-NLOS}(d_{3D}))$ $PL_{UMi-NLOS}=35.3\log_{10}(d_{3D}) + 22.4 + 21.3\log_{10}(f_c) - 0.3(h_{UE} - 1.5)$ **Option: CI model with 1m reference distance:** $PL = 32.4 + 20\log_{10}(f_c) + 31.9\log_{10}(d_{3D})$	$\sigma_{SF} = 7.82$ $\sigma_{SF} = 8.2$	$f_c = 28GHz$ $10m < d_{2D} < 5000m$ $1.5m < h_{UE} < 22.5m$ $h_{BS} = 10m$
	METIS	LOS	$PL_{UMi-LOS} = \begin{cases} PL_1, & 10m < d_{3D} \le d_{BP} \\ PL_2, & d_{BP} < d_{3D} < 500m \end{cases}$ $PL_1 = 22\log_{10}(d_{3D}) + 28.0 + 20\log_{10}(f_c) + PL_0$ $PL_2 = 40\log_{10}(d_{3D}) + 7.8 - 18\log_{10}(h_{BS}h_{UE}) + 2\log_{10}(f_c) + PL_1(d_{BP})$	$\sigma_{SF} = 3.1$	$f_c = 28GHz$ $10m < d_{2D} < 5000m$ $h_{BS} = 10m$ $1.5m < h_{UE} < 22.5m$
	mmMAGIC	LOS	$PL = 19.2\log_{10}(d_{3D}) + 32.9 + 20.8\log_{10}(f_c)$	$\sigma_{SF} = 2.0$	$f_c = 28GHz$
		NLOS	$PL = 45.0\log_{10}(d_{3D}) + 31 + 20.0\log_{10}(f_c)$	$\sigma_{SF} = 7.82$	$f_c = 28GHz$

Table 3.1 Path Loss Models IN UMi Street Canyon Scenario

			PL [dB], f_c is in GHz and d_{3D} is in meters	Shadow fading std [dB]	Applicability range and Parameters
Umi-Open Square	5GCM	LOS	**CI model with 1 m reference distance:** $PL = 32.4 + 18.5\log_{10}(d_{3D}) + 20\log_{10}(f_c)$	$\sigma_{SF} = 4.2$	$f_c = 28GHz$
		NLOS	**CI model with 1m reference distance:** $PL = 32.4 + 28.9\log_{10}(d_{3D}) + 20\log_{10}(f_c)$ **ABG model:** $PL = 41.4\log_{10}(d_{3D}) + 3.66 + 24.3\log_{10}(f_c)$	$\sigma_{SF} = 7.1$ $\sigma_{SF} = 7.0$	$f_c = 28GHz$

Table 3.2 Path Loss Models IN UMi Open Square Scenario

Comparisons among the different path loss models including LOS and NLOS described here are provided in Figure 3.1.
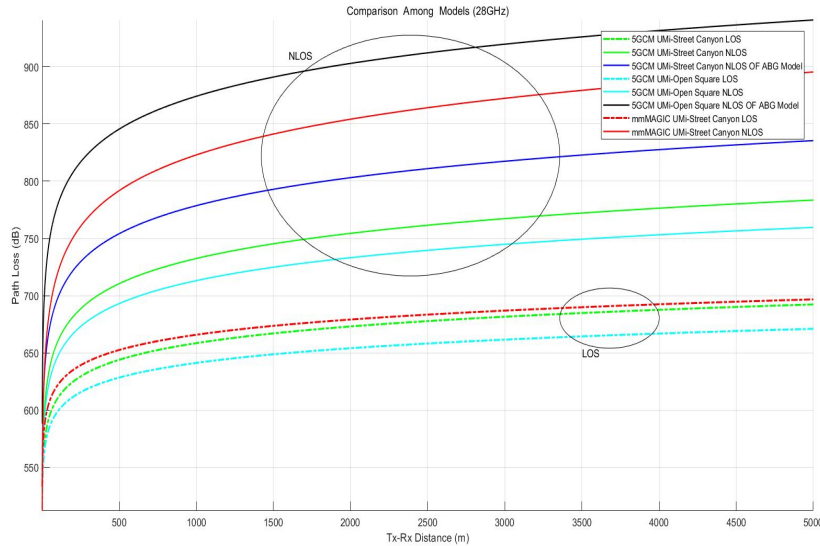
Figure 3.1: Comparisons among the different path loss models

3.2.2 UMa Path Loss

The following models are suitable for 28 GHz measurements in UMa scenario[23]. 5GCM: There are three UMa path loss models for: CI, CIF and ABG. The PLE for the CI/CIF model of UMa is slightly lower than the UMi model, indicating less distance loss, which is intuitive and meaningful, because a larger BS height means fewer obstacles are encountered than in a UMi scenario (see parameter Table 3.1). 3GPP TR 38.901: For the UMa NLOS scenario, an ABG model and an optional CI model are provided (see parameter table 3.3).

3.3 Indoors: Indoor-Office and Shopping-Mall

For the application models of 28GHz in indoor scenario, the measurement models of three organizations are mainly introduced. In

		PL [dB], f_c is in GHz and d_{3D} is in meters	Shadow fading std [dB]	Applicability range and Parameters
UMa	5GCM	LOS	**CI model with 1 m reference distance:** $PL = 32.4 + 20\log_{10}(d_{3D}) + 20\log_{10}(f_c)$	$\sigma_{SF} = 4.1$	$f_c = 28GHz$
		NLOS	**CI model with 1m reference distance:** $PL = 32.4 + 30\log_{10}(d_{3D}) + 20\log_{10}(f_c)$ **ABG model:** $PL = 34\log_{10}(d_{3D}) + 19.2 + 23\log_{10}(f_c)$	$\sigma_{SF} = 6.8$ $\sigma_{SF} = 6.5$	$f_c = 28GHz$
	3GPP TR 38.901	LOS	$PL_{UMa-LOS} = \begin{cases} PL_1, & 10m \le d_{2D} \le d'_{BP} \\ PL_2, & d'_{BP} \le d_{2D} \le 5km \end{cases}$ $PL_1 = 28.0 + 22\log_{10}(d_{3D}) + 20\log_{10}(f_c)$ $PL_2 = 28.0 + 40\log_{10}(d_{3D}) + 20\log_{10}(f_c)$ $\quad -9\log_{10}((d'_{BP})^2 + (h_{BS} - h_{UE})^2)$ where $d'_{BP} = 4 h'_{BS} h'_{UE} f_c * 10^9/c$	$\sigma_{SF} = 4.0$	$f_c = 28GHz$ $1.5m < h_{UE}$ $< 22.5m$ $h_{BS} = 25m$
		NLOS	$PL = \max(PL_{UMa-LOS}(d_{3D}), PL_{UMa-NLOS}(d_{3D}))$ $PL_{UMa-NLOS} = 13.5 + 39.08\log_{10}(d_{3D}) + 20\log_{10}(f_c)$ $\quad - 0.6(h_{UE} - 1.5)$ **Option: CI model with 1m reference distance:** $PL = 32.4 + 20\log_{10}(f_c) + 30\log_{10}(d_{3D})$	$\sigma_{SF} = 6.0$ $\sigma_{SF} = 7.8$	$f_c = 28GHz$ $10m < d_{2D}$ $< 5000m$ $1.5m < h_{UE}$ $< 22.5m$ $h_{BS} = 25m$

Table 3.3 Path Loss Models IN UMa Scenario

the 5GCM InH scenario [23], in addition to the CI, CIF and ABG path loss models, a dual-slope path loss model for different distance regions in the propagation environment is proposed, as shown in Table 3.4. InH-Office considers a single-slope CIF model that uses only two optimization parameters, while the double slope model may be best suited for shopping malls or large indoor distances，which are greater than 50 meters. The 3GPP TR 38.901 InH-office is slightly lower than the PLE in the UMi Street Canyon because the reflection and scattering of walls and ceilings in the indoor environment is more, and the waveguide effect on the corridor increases the received signal power. The NLOS path loss model has no height correction and requires a patch to ensure it is limited by the LOS path loss which is given in Table 3.4. The InH channel model in mmMAGIC uses an earlier version of 5GCM in the same form as the ABG model. For indoor NLOS, the value of the path loss model parameter has been averaged from InH and InH-Shopping Mall (Table 3.5).

3.4 O2I penetration Loss

Considering the building penetration loss (BPL) at the 28 GHz, the O2I path loss model is according to 3GPP TR 38.901 [23], and has the following form:

$$PL \, [dB] = PL_b + PL_{tw} + PL_{in} + N(0, \sigma P2) \quad (22)$$

where PL_b is the basic outdoor path loss, PL_{tw} is the BPL through the outer wall, PL_{in} is the indoor loss, it depends on the depth of entering the building, and σ_P is the standard deviation of the penetration loss. The BPL PL_{tw} can be modeled as

$$PL_{tw}[dB] = PL_{npi} - 10\log_{10} \sum_{i=1}^{N} (p_i * 10^{\frac{L_{material_i}}{-10}})$$

where PL_{npi} is an additional loss, plus external wall loss to resolve non-

	PL [dB], f_c is in GHz and d_{3D} is in meters	Shadow fading std [dB]	Applicability range and Parameters
Indoor-Office — LOS	**CI model with 1 m reference distance:** $$PL = 32.4 + 17.3\log_{10}(d_{3D}) + 20\log_{10}(f_c)$$	$\sigma_{SF} = 3.02$	$f_c = 28GHz$
NLOS Single slope (FFS)	**CIF:** $$PL = 32.4 + 31.9\left(1+0.06\left(\frac{f_c - 24.2}{24.2}\right)\right)\log_{10}(d_{3D}) + 20\log_{10}(f_c)$$ **ABG model:** $$PL = 38.3\log_{10}(d_{3D}) + 17.30 + 24.9\log_{10}(f_c)$$	$\sigma_{SF}^{CIF} = 8.29$ $\sigma_{SF}^{ABG} = 8.03$	$f_c = 28GHz$
5GCM — NLOS dual slope (FFS)	**Dual-Slope CIF model:** $$PL_{Dual}^{CIF}(d) = \begin{cases} FSPL(f_c,1m) + 10n_1\left(1+b_1\left(\frac{f_c-f_0}{f_0}\right)\right)\log_{10} d, & 1 < d \le d_{BP} \\[2ex] FSPL(f_c,1m) + \\ 10n_1\left(1+b_1\left(\frac{f_c-f_0}{f_0}\right)\right)\log_{10}(d_{BP}) + 10n_2\left(1+b_2\left(\frac{f_c-f_0}{f_0}\right)\right)\log_{10}\left(\frac{d}{d_{BP}}\right), & d > d_{BP} \end{cases}$$ **Dual-Slope ABG model:** $$PL_{Dual}^{ABG}(d) = \begin{cases} \alpha_1.10\log_{10}(d)+\beta_1+\gamma.10\log_{10}(f_c), & 1 < d \le d_{BP} \\[2ex] \alpha_1.10\log_{10}(d_{BP})+\beta_1+\gamma.10\log_{10}(f_c)+\alpha_2.10\log_{10}\left(\frac{d}{d_{BP}}\right), & d > d_{BP} \end{cases}$$	$\sigma_{SF}^{CIF} = 7.65$ $\sigma_{SF}^{ABG} = 7.78$	$f_c = 28GHz$ **Dual-Slope CIF model:** $n_1 = 2.51, b_1 = 0.12$ $f_0 = 24.1GHz, n_2 = 4.25$ $b_2 = 0.04, d_{BP} = 7.8m$ **Dual-Slope ABG model:** $\alpha_1 = 1.7, \beta_1 = 33.0$ $\gamma = 2.49, d_{BP} = 6.9m$ $\alpha_2 = 4.17$

Table 3.4 Path Loss Models IN Indoor office Scenario

		PL	σ_{SF}	
3GPP TR 38.901	LOS	$PL_{InH-LOS} = 32.4 + 17.3\log_{10}(d_{3D}) + 20\log_{10}(f_c)$	$\sigma_{SF} = 3.0$	$f_c = 28GHz$ $1 \leq d_{3D} \leq 100m$
	NLOS	$PL = \max(PL_{InH-LOS}(d_{3D}), PL_{InH-NLOS}(d_{3D}))$ $PL_{InH-NLOS} = 17.30 + 38.3\log_{10}(d_{3D}) + 24.9\log_{10}(f_c)$ **Option: CI model with 1m reference distance:** $PL = 32.4 + 20\log_{10}(f_c) + 31.9\log_{10}(d_{3D})$	$\sigma_{SF} = 8.03$ $\sigma_{SF} = 8.29$	$f_c = 28GHz$ $1 \leq d_{3D} \leq 86m$ $1 \leq d_{3D} \leq 86m$
mmMAGIC	LOS	$PL = 13.8\log_{10}(d_{3D}) + 33.6 + 20.3\log_{10}(f_c)$	$\sigma_{SF} = 1.18$	$f_c = 28GHz$
	NLOS	$PL = \max(PL_{LOS}(d_{3D}), PL_{NLOS}(d_{3D}))$ $PL = 36.8\log_{10}(d_{3D}) + 15.2 + 26.8\log_{10}(f_c)$	$\sigma_{SF} = 8.03$	$f_c = 28GHz$

Table 3.4 Path Loss Models IN Indoor office Scenario

Table 3.5 Path Loss Models IN Shopping Mall Scenario

		PL [dB], f_c is in GHz and d_{3D} is in meters	Shadow fading std [dB]	Applicability range and Parameters
Shopping -Mall	LOS	**CI model with 1 m reference distance:** $PL = 32.4 + 17.3\log_{10}(d_{3D}) + 20\log_{10}(f_c)$	$\sigma_{SF} = 2.01$	$f_c = 28GHz$
	NLOS Single slope (FFS)	**CIF model:** $PL = 32.4 + 25.9(1 + 0.01(\frac{f_c - 39.5}{39.5}))\log_{10}(d_{3D}) + 20\log_{10}(f_c)$ **ABG model:** $PL = 32.1\log_{10}(d_{3D}) + 18.09 + 22.4\log_{10}(f_c)$	$\sigma_{SF}^{CIF} = 7.40$ $\sigma_{SF}^{ABG} = 6.97$	$f_c = 28GHz$
5GCM	NLOS dual slope (FFS)	**Dual-Slope CIF model:** $$PL_{Dual}^{CIF}(d) = \begin{cases} FSPL(f_c, 1m) + 10n_1(1 + b_1\left(\frac{f_c - f_0}{f_0}\right))\log_{10} d\,, 1 < d \leq d_{BP} \\ FSPL(f_c, 1m) + \\ 10n_1\left(1 + b_1\left(\frac{f_c - f_0}{f_0}\right)\right)\log_{10}(d_{BP}) + 10n_2\left(1 + b_2\left(\frac{f_c - f_0}{f_0}\right)\right)\log_{10}(\frac{d}{d_{BP}}) \\ \qquad\qquad, d > d_{BP} \end{cases}$$ **Dual-Slope ABG model:** $$PL_{Dual}^{ABG}(d) = \begin{cases} \alpha_1. 10\log_{10}(d) + \beta_1 + \gamma. 10\log_{10}(f_c), 1 < d \leq d_{BP} \\ \alpha_1. 10\log_{10}(d_{BP}) + \beta_1 + \gamma. 10\log_{10}(f_c) + \alpha_2. 10\log_{10}\left(\frac{d}{d_{BP}}\right), d > d_{BP} \end{cases}$$	$\sigma_{SF}^{CIF} = 6.26$ $\sigma_{SF}^{ABG} = 6.36$	$f_c = 28GHz$ **Dual-Slope CIF model:** $n_1 = 2.43, b_1 = -0.01$ $f_0 = 39.5GHz, n_2 = 8.36$ $b_2 = 0.39, d_{BP} = 110m$ **Dual-Slope ABG model:** $\alpha_1 = 2.9, \beta_1 = 22.17$ $\gamma = 2.24, d_{BP} = 147.0m$ $\alpha_2 = 11.47$

	Path loss through external wall; PL_{tw} [dB], f_c is in GHz and d is in meters	Indoor loss: PL_{in} [dB], d is in meters	Standard deviation σ_p[dB]
3GPP TR 38.901 Low-loss model	$5 - 10\log_{10}\left(0.3 * 10^{-\frac{L_{glass}}{10}} + 0.7 * 10^{-\frac{L_{concrete}}{10}}\right)$	$0.5 d_{2D-in}$	4.4
3GPP TR 38.901 High-loss model	$5 - 10\log_{10}\left(0.7 * 10^{-\frac{L_{IRRglass}}{10}} + 0.3 * 10^{-\frac{L_{concrete}}{10}}\right)$	$0.5 d_{2D-in}$	6.5

Table 3.6 O2I PENETRATION LOSS PARAMETERS

Material	Penetration loss[dB], f_c is in GHz
Standard multi-pane glass	$L_{glass} = 2 + 0.2 * f_c$
IRR glass	$L_{IRRglass} = 23 + 0.3 * f_c$
Concrete	$L_{concrete} = 5 + 4 * f_c$
Wood	$L_{wood} = 4.85 + 0.12 * f_c$

Table 3.7 O2I PENETRATION LOSS OF DIFFERENT MATERIALS

symmetric normal incidence, f_c is the material's penetration loss i, f_c is the frequency in GHz, and p_i is the ratio of the i th material, where $\sum p_i = 1$, and N is the number of materials. Table 3.7 shows the permeability loss and O2I permeation loss models for several materials.

Chapter 4

4.1 Base station

4.1.1 Coverage Area

A cellular network is a radio network distributed over land areas called cells, each served by at least one fixed-location transceiver known as a cell site or base station. These cells joined together provide radio coverage over a large geographic area. This radio network enables many portable transceivers (e.g., mobile phones, pagers, etc.) to communicate with each other and with fixed transceivers and telephones anywhere in the network, via base stations, even if some of the transceivers are moving through more than one cell during transmission. The cell and network coverage depend mainly on natural factors such as geographical aspect/propagation conditions, and on human factors such as the landscape (urban, suburban, rural), subscriber behavior etc. The ultimate quality of the coverage in the mobile network is measured in terms of location probability. The BS coverage area [24] depends on their capacity, the height of the antennae, the frequency range of radiated signals, the density of development of the territory.

4.1.2 Link Budget and its Calculations

The link budget of a communication system depends mainly on the

base station and the mobile station's specifications. The link budget looks at the elements that will determine the signal strength arriving at the receiver. Link budget calculations are used for calculating the power levels required for cellular communications systems, and for investigating the base station coverage.

The link budget includes the following parameter.

- Transmitter power.
- Antenna gains (both transmitter antenna gain and receiver antenna gain).
- Antenna feeder losses.
- Path loss
- Receiver sensitivity

In order to formulate a link budget equation, it is required to investigate all the areas where gains and losses may occur between the transmitter and the receiver.

Received power (dBm) = Transmitted power (dBm) + gains (dBm) - losses (dBm)   (4.1)

In basic calculation of link budget equation, it is assumed that the power spreads out equally in all directions from the transmitter source. A typical link budget equation for a radio communications system may look like the following:

$$P_{RX} = P_{TX} + G_{TX} + G_{RX} - L_{TX} - L_{FS} - L_{FM} - L_{RX} \qquad (4.2)$$

Where:

- P_{RX} = received power (dBm)
- P_{TX} = transmitter output power (dBm)
- G_{TX} = transmitter antenna gain (dBi)
- G_{RX} = receiver antenna gain (dBi)
- L_{TX} = transmit feeder and associated losses (feeder, connectors, etc.) (dB)
- L_{FS} = free space loss or path loss (dB)

36

- L_{FM} = many-sided signal propagation losses (these include fading margin, polarization mismatch, losses associated with medium through which signal is travelling, other losses...) (dB)

- L_{RX} = receiver feeder losses (feeder, connectors, etc.) (dB)

EIRP is the measure of power in specific direction, which is related to the transmitted power (P_{TX}), the transmission losses L, and the antenna gain (G_{TX})

$$EIRP = P_{TX} - L + G \qquad (4.3)$$

The objective of power budget calculation is to balance the uplink and down link. The receive signal sensitivity may be different because the mobile station and the base transceiver station has different Radio frequency architecture. The power of BTS can be adjusted to balance the whole link. The power balance (uplink and down link) decide the cell range.

4.1.3 Products

Anokiwave offers a uniquely positioned product portfolio for the 5G, RADAR and SATCOM markets with professional system level understanding and the best technology choices [25]. For 28 GHz, there are two products shown in Table 4.1. Both two products are active array for 5G wireless applications developed using planar antenna technology with minimal form factor and light weight, which lead network operators in the use of the mmWave band to show how 5G coverage, with low power consumption and high energy efficiency while meeting key operating specifications for data rate, delay, coverage and reliability.

Market	Band	Product Family	Part Number	Freq. Range	Tx Pwr	Rx NF	Package	Description
Active Antenna Innovator Kits	28 GHz	Active Antenna	AWMF-0129	27.5 - 30.0 GHz	–	–	Planar Active Antenna	64 Element Innovator Kit
			AWA-0134	27.5 - 30.0 GHz	–	–		256 Element Innovator Kit

Table 4.1 Anokiwave products in the use of 28 GHz

The surface of the AWMF-0129 Mounted Antenna Board is based on Anokiwave's AWMF-0108 silicon quad-core IC, demonstrating the performance achievable with low power silicon integration and efficient antenna layout and design (see Figure 4.1). Using the AWMF-0108, the antenna provides +50dBmi of output power while consuming only 12W of DC power in the RF circuit and achieving Gb / s data rates in the OTA tests. Electronic 2D beam steering is achieved using analog RF beamforming with independent phase and gain control in both Tx and Rx modes of operation. Performance of AWMF-0129 are given as following:

- 27.5-30 GHz operation
- Tx/Rx half duplex operation
- +50 dBmi EIRP at P1dB
- -7 dB/K G/T (receiver sensitivity)
- Vertical linear polarization
- 2D electronic beam scan
- Programmable beam widths
- Temperature sense telemetry
- Fast beam update rate
- 0.5 kg weight
- 11 x 15 x 4 cm size
- 18 W DC average power

Figure 4.1 AWMF-0129 5G 28 GHz Active Antenna Innovator's Kit

The AWA-0134's surface is also fitted with an assembled antenna board based on Anokiwave's AWMF-0108, which is shown in Figure 4.2. With the AWMF-0108, the antenna provides 60 dBmi (1000 W) EIRP. Electronic 2D beam steering is achieved using analog RF beamforming with independent phase and gain control in both Tx and Rx modes of operation. Performance of AWMF-0129 are shown as following:

- 26.5–29.5 GHz operation
- 256–element single beam or 4 x 64–element MU-MIMO operation
- Tx/Rx half duplex operation
- Linear polarization
- 2D electronic beam scan
- Programmable beam widths
- 4 Pre-programmed beam states:

  Uniform Illumination; 25dB SLL Taylor taper plus two broad beams for broadcast
- Temperature sense telemetry
- Passive cooling option
- Suitable for outdoor deployment

Figure 4.2 AWA-0134 5G 28 GHz 256-Element Active Antenna Innovator's Kit

4.2 Mobile Terminal

4.2.1 Introduction

A mobile communication device is a small, portable electronic device, with wireless communication capabilities, which is easy to carry around. A mobile phone, which is also known as mobile terminal (MT) [26] , cellular phone, cell phone, hand phone, or simply a phone, is a device that can send and receive telephone calls over a radio link while being connected to a cellular base station operated by a cellular network operator. Mobile terminal modem unit interfaces with the cellular base stations and sends/receives user information generated by the application unit.

4.2.2 Minimum detectable signal

A minimum detectable signal is a signal at the input of a system whose power produces a signal-to-noise ratio of m at the output and the name sensitivity is used for this concept. The minimum detectable signal is a specific value of the minimum receivable power (Pr_{min}) [27]. The minimum detectable signal is defined as the useful echo power at the antenna, which gives a signal at the output of the IF amplifier (just

before detection). To establish the minimum detectable signal (MDS) of a receiver we require several factors to be known:

- Required signal-to-noise ratio (SNR) in dB
- Detection bandwidth (BW) in Hz
- Temperature of the receiver system T0 in kelvins
- Boltzmann's constant k = 1.38×10−23 joules per kelvin
- Receiver noise figure (NF) in dB

The signal is 3 dB above the average noise level and is shown in Figure 4.3. MDS is usually expressed in dBm; typical values are between -100 and -103 dBm.
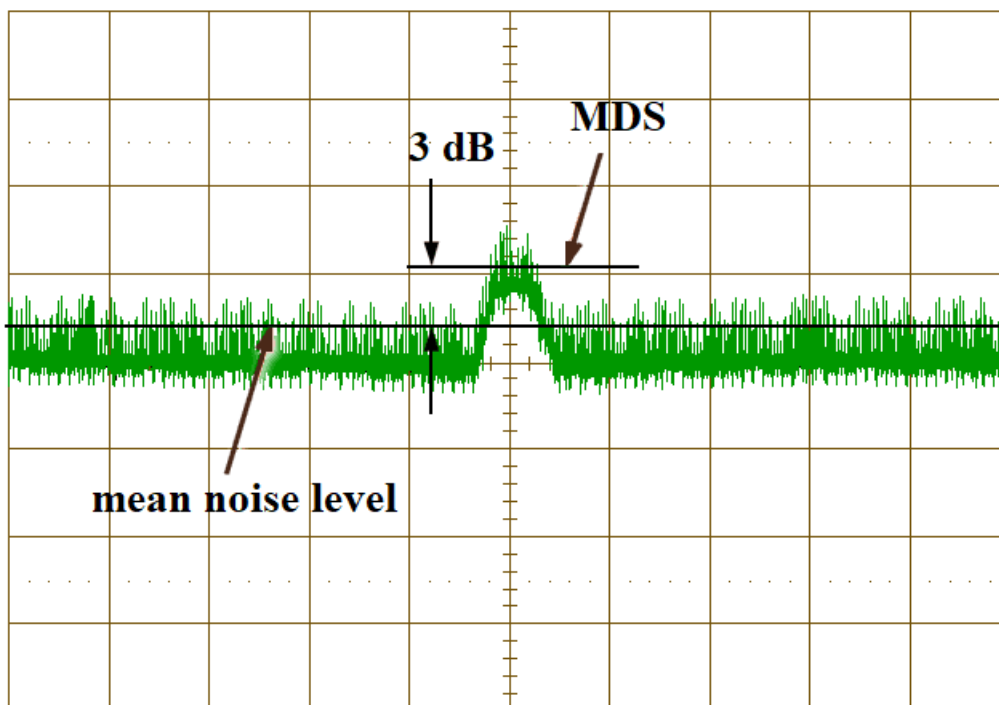
Figure 4.3 The signal is 3 dB above the average noise level

4.3 Integrated Access Backhaul in Millimeter Wave Networks

In the workshop on "A close look to 5G network technology", Huawei presented IAB to make mmWave mobile 5G possible [28], and showed that IAB provides: Coverage extension, Incremental network

deployment, Capacity enhancement (e.g., in traffic hotspots), Coverage gap filling (see Figure 4.4).
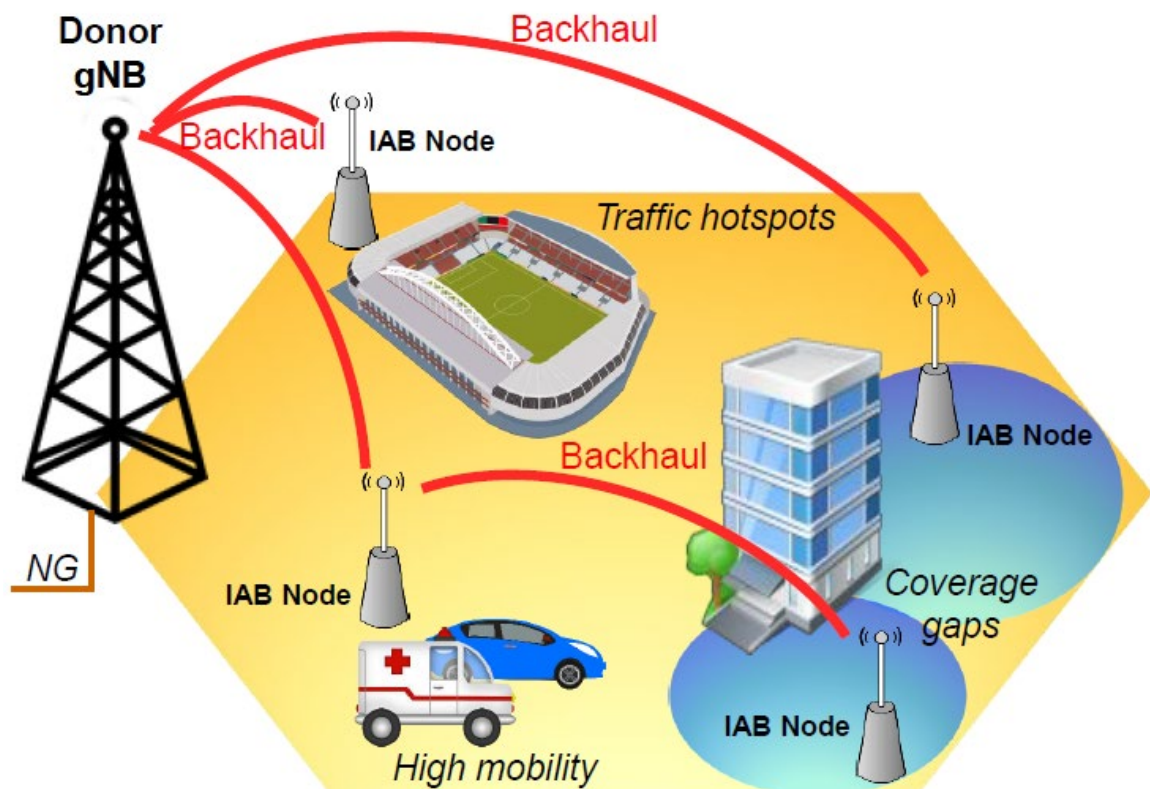

Figure 4.4 The application of Integrated access backhaul

Integrated access backhaul (IAB) [29], where the summation of the allotted bandwidth among access and backhaul links if fixed, can dynamically change the partition between access and backhaul links and meet instantaneous demand of UEs across the network. IAB can significantly reduce the fiber drop deployment cost of the network compared to fixed access backhaul network. IAB can also provide seamless integration between access and backhaul links. IAB using mmW band is especially advantageous because mmW links tend to be noise limited due to the directional nature of interference. Non-adjacent access and backhaul links can share the same bandwidth without interference. Integrated access and backhaul communications use the same standard radio technology (e.g. 5G NR), allows interoperability

among base stations from different manufacturers, which is essential for flexible deployment of dense small cell networks. IAB can be deployed through both in-band and out-band relaying and used in both indoor and outdoor networks.

According to [30], NR cellular networks with IAB functionalities will be characterized by (i) the possibility of using the mmWave spectrum; (ii) the integration of the access and backhaul technologies, i.e., using the same spectral resources and infrastructures to serve both mobile terminals in access as well as the NR gNBs in backhaul [26]; (iii) a higher flexibility in terms of network deployment and configuration with respect to LTE, i.e., the possibility of deploying plug-and-play IAB nodes capable of self-configuring and self-optimizing themselves. According to [30], 5G IAB relays will be used in both outdoor and indoor scenarios, possibly with multiple wireless hops, with the final goal of extending the coverage of cell-edge users, avoiding service unavailability, and increasing the efficiency of the resource allocation. Both in-band and out-of-band backhaul will be considered, with the first being a natural candidate for a tighter integration between access and backhaul.
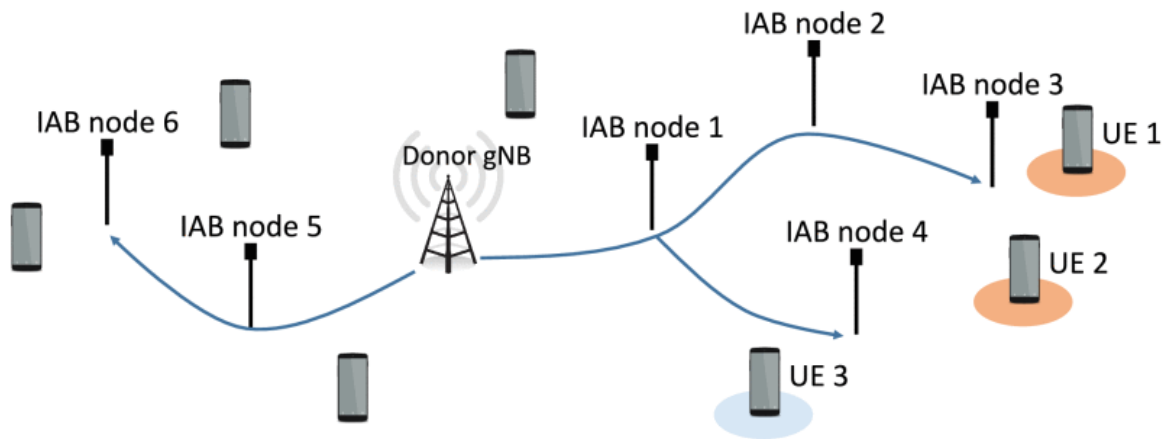
Figure 4.5 Example of IAB architecture, with a single donor and multiple downstream IAB nodes.

According to the deployment in Figure 4.5 [31] and present a possible resource partitioning for the donor gNB, IAB nodes 1, 2 and 3 and the UEs connected to these gNBs. As can be seen, each IAB node does not allocate access transmission in the resources reserved for it backhaul but can exploit all of the other resources for communication with other relays and the UEs, including those allocated by one of the upstream nodes to other backhaul links. Advantages and Disadvantages of Integrated Access Backhaul are conclude as following:

The Advantages are:

- Higher spectrum efficiency
- Reuse of time, frequency and space resources between access and backhaul
- Higher cost efficiency
- Sharing the same radio hardware unit
- Sharing same O&M systems, simplifying system management
- Higher Performance
- Lower latency (Receive and Forward simultaneously)
- Dynamic optimization of resource across access and backhaul

The disadvantages are:

- A new type of interference (access backhaul interference) to mitigate

- Complex scheduling of the channel resources (across two domains, access and backhaul)

- Potential limitations on the end user experience (e.g. rate, latency) due to the sharing of resources between access and backhaul

- Regulatory framework for spectrum rules may not be in place

Islam, M. N., et al. [29] used Table 4.2 which lists the simulation parameters to generate simulation results. There are eighteen base stations in the network. The average inter site distance is 200 m. 600 UEs are randomly thrown into the streets of this scenario. UEs are associated with the base station based on maximum signal strength. The link gains between UEs and base stations are obtained from a ray tracing tool named WINPROP.

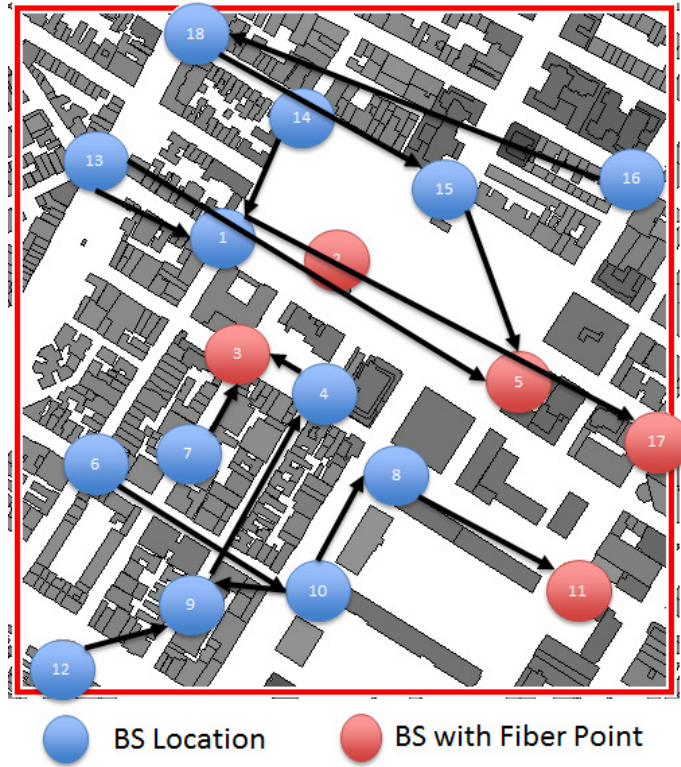| Parameter	Value
BS Tx Power (dBm)	30
BS array	16×8
Array gain (dB)	21
BS EIRP (dBm)	51
Total bandwidth (GHz)	1
Frequency (GHz)	28
Atmospheric absorption (dB/km)	0.11
Polarization loss (dB)	1
Alignment error (dB)	5
Implementation loss (dB)	5

Table 4.2   Link budget calculation

Figure 4.6: Network connectivity in IAB solution. Five fiber drops are required to meet 25 Mbps DL and UL demand of each UE.
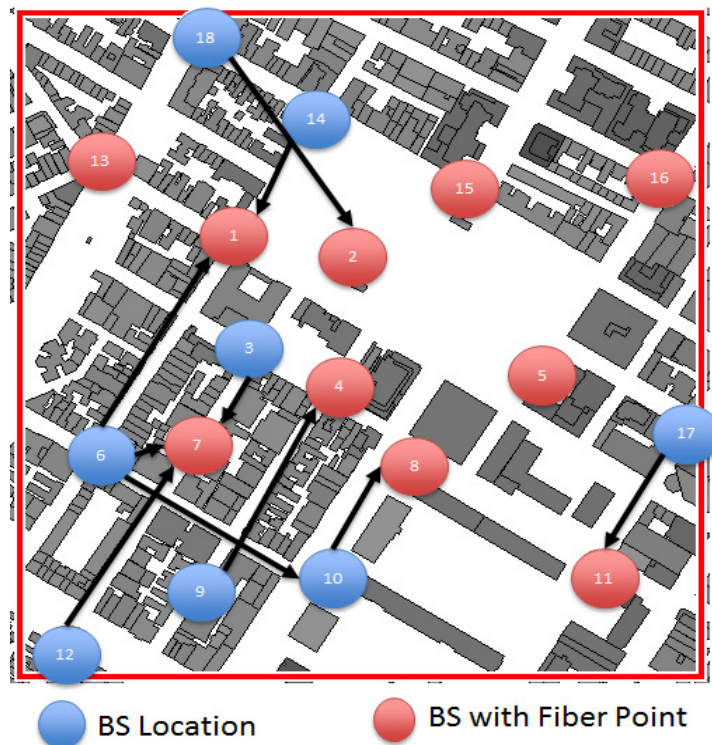

Figure 4.7: Network connectivity in fixed access backhaul solution. Ten fiber drops are required to meet 25 Mbps DL and UL demand of each UE

Figure 4.6 shows the network connectivity in an IAB network and shows that only five fiber drops are required to meet 25 Mbps DL and UL demand from each UE. Figure 4.7 shows the network connectivity in a fixed access backhaul network. Ten fiber drops are required among eighteen base stations to meet 25 Mbps DL and UL demand from each UE. Fig. 4.6 and Fig. 4.7 suggests that the number of required fiber drops in IAB is half than that in a fixed access backhaul. The advantage of IAB can be explained by focusing on base station index 2. Base station 2 is placed in a relatively open place compared to other base stations.
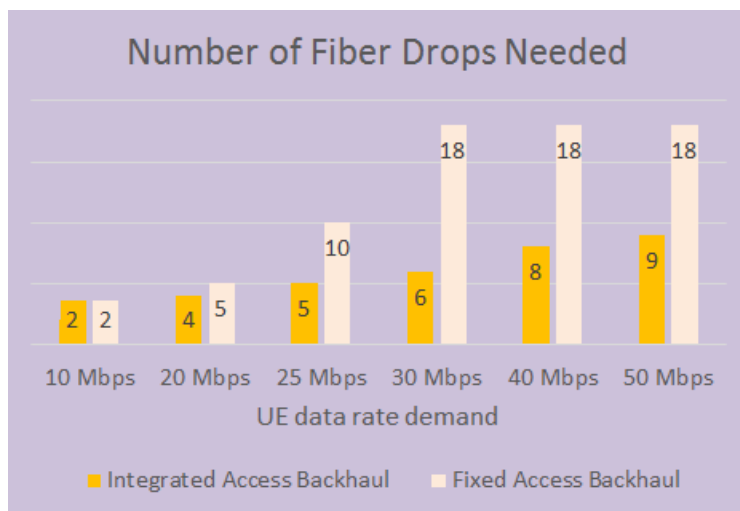

Figure 4.8: Required number of fiber drops in IAB and Fixed access backhaul network

Figure 4.8 compares the performance of integrated access backhaul and fixed access backhaul networks for different user demands. Fig. 4 shows that IAB reduces the number of fiber drop deployment significantly throughout the network.

Fixed access backhaul splits the total resource to access and backhaul links in a fixed manner throughout the network and cannot meet a sudden increase in demand in some parts of the network. Integrated access backhaul (IAB) – where the summation of the allotted

bandwidth among access and backhaul links if fixed can meet dynamic traffic demand by splitting the threshold for access and backhaul bandwidth differently at different nodes of the network. Therefore, IAB can significantly reduce the fiber deployment cost or increase the utility of a small cell wireless network that operates at mmW band.

Chapter 5

Coverage Simulations

5.1 Probability of Line-of-Sight

The mobile industry has found the benefits of path loss describing the LOS and NLOS conditions, respectively. Therefore, a model for LOS probabilities is needed, i.e. a statistical model is needed to predict the likelihood of the UE being within the explicit LOS of the BS or within the NLOS region due to obstacles.

The probability of LOS corresponds to the probability that radiation from the transmitter (TX) will not be blocked by buildings or other obstructions, traveling along a straight and unobstructed propagation path in the urban environment (i.e., zero reflections) to the receiver (RX). Similarly, the NLOS probability corresponds to the probability that the radiation will be obstructed by at least one object, and travel along an obstructed path to reach the RX (i.e., via scattering, or from one or more reflections). These two probabilities heavily depend upon the physical, site-specific environment in which the TX and RX are located.

LOS probability curves from raytracing as a function of T-R separation distance for TX locations. The mean LOS probability was computed from the four distinct LOS probability curves from the four physical TX locations used in [32] and [33]. The mean LOS probability curve was fit to an analytical function of the form [34]:

$$P_{LOS}(d) = \left[\min\left(\frac{d_{BP}}{d}, 1\right)\left(1 - e^{-\frac{d}{\alpha}}\right) + e^{-\frac{d}{\alpha}}\right]^2$$

where d_{BP} is the breakpoint distance at which the LOS probability is no longer equal to 1, and α (m) is a decay parameter. In this work, we applied the minimum mean square error (MMSE) method, which yielded values of d_{BP} = 27 m and α = 71 m that minimize the mean square error between the mean LOS curve in Figure 5.1
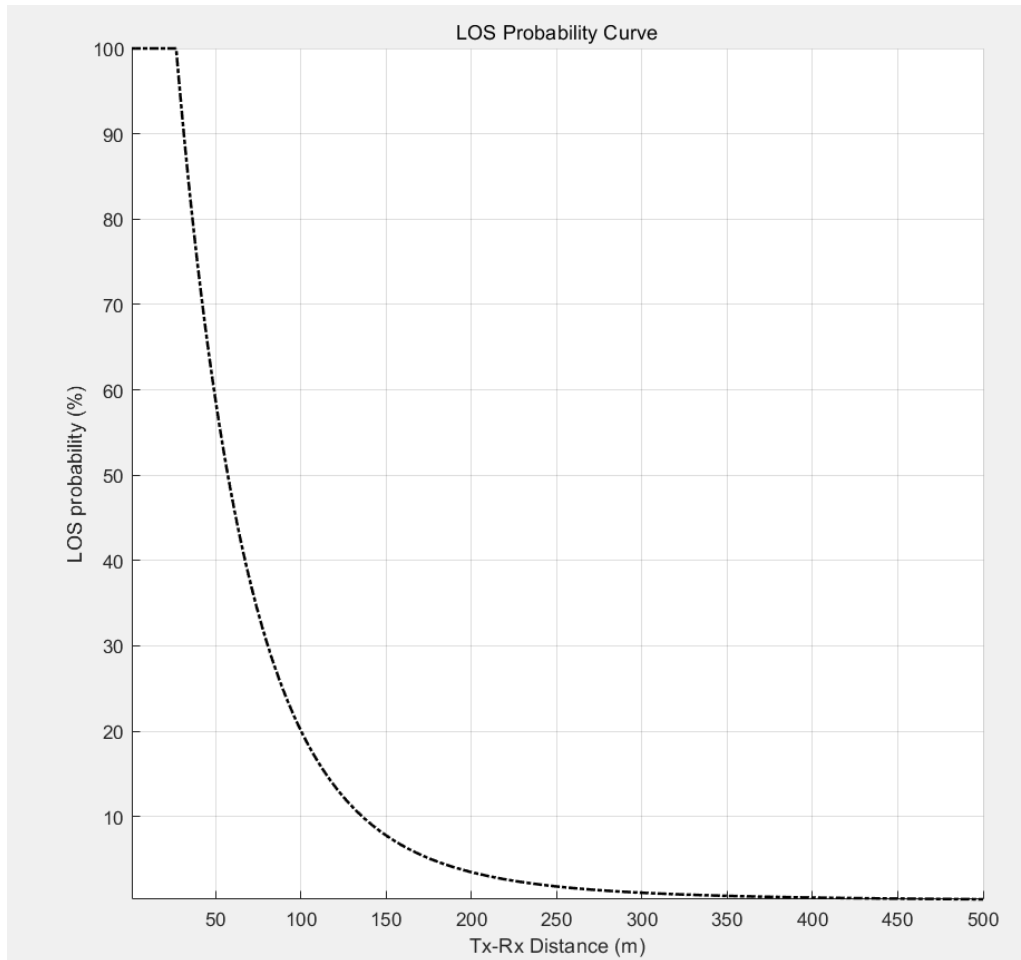

Figure 5.1: The mean LOS probability curve was obtained by averaging the four LOS probability curves

As the T-R separation distance increases from 10 m to about 30 m, the probability of LOS remains constant with a value of 100%, and decreases monotonically after 30 m, as the environment becomes denser with more path obstructions.

50

5.2 Simulation results

The simulation is performed at 28 GHz for an elevation area of 1000x1000 m^2 and then generates users with a random position. By applying a random generator to determine whether the user is LOS or NLOS, a random number in range of [0,1] with a uniform distribution is generated. Fig.5.2 shows the coverage of one base station, shown in blue circle at the center of the area. There are approximately 1000 users in the network, shown in blue asterisks are covered by BS and in red asterisks are not covered. As shown in the figure, distances between the TX and RX ranged from10 m to 100 m, the probability of LOS is higher than the value of 20%.
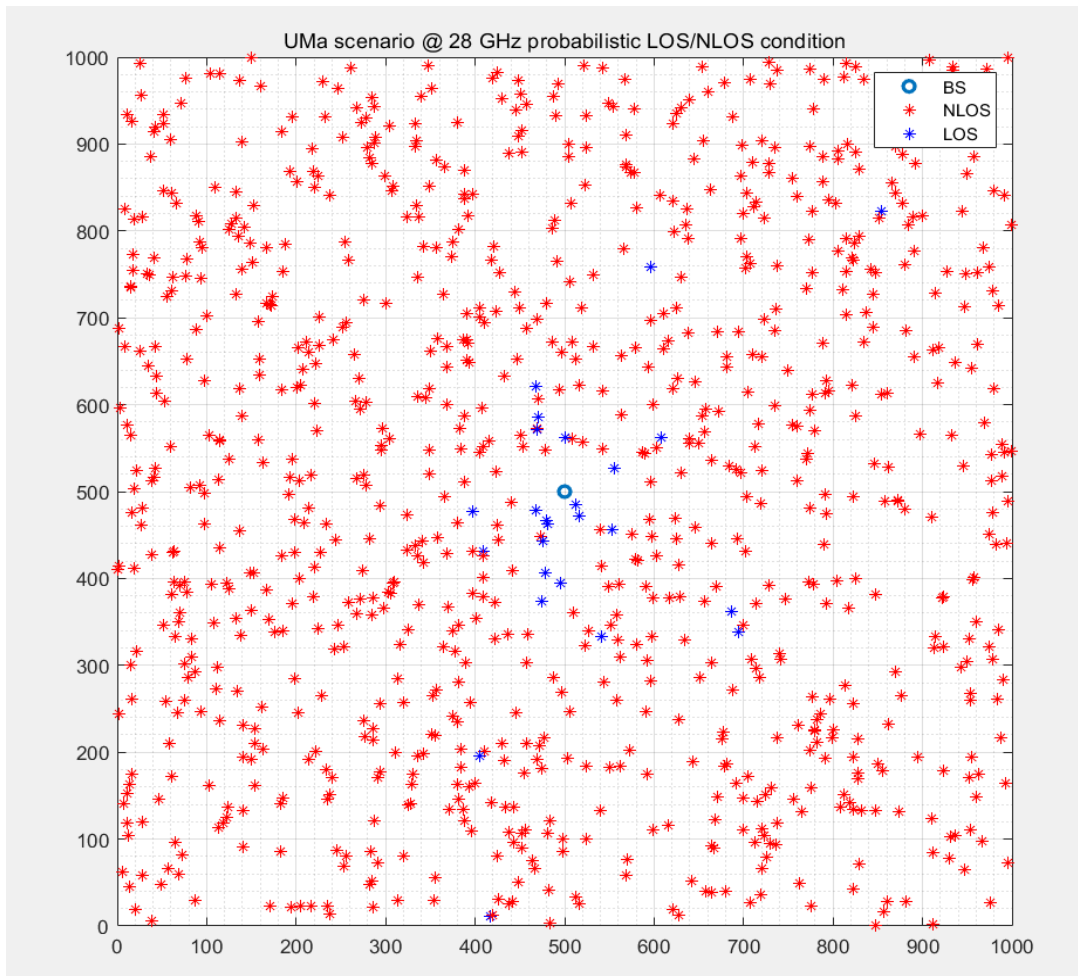

Figure 5.2: Coverage of one base station in UMa scenario of 28 GHz under probabilistic LOS/NLOS condition

Chapter 6

Conclusions

MmWave band play an important role in the 5G wireless technologies. As is known to all there are many companies and research groups have proposed measurements and models focusing on the band of 28 GHz. MmWave will need to utilize and quickly adapt to the spatial dynamics of the wireless channel as larger gain antennas will be used to overcome path loss. It is meaningful to describe the path loss for the LOS and NLOS conditions, respectively. LOS propagation will offer more reliable performance in mmWave communications as compared to NLOS conditions, given the greater diffraction loss at higher frequencies, and given the larger path loss exponent (PLE) as well as increased shadowing variance in NLOS as compared to LOS. The model for the LOS probability was simulated, which can predict the likelihood that a UE is within the explicit LOS of the BS or in an NLOS region due to obstructions. As the T-R separation distance increases from 10 meters to about 30 meters, the probability of LOS remains constant, with a value of 100%, and as the environment becomes denser, the path barriers increase, monotonously decreasing after 30 meters.

Bibliography

[1] J. S. Seybold, Introduction to RF propagation: John Wiley & Sons, 2005.

[2] A. Osseiran, F. Boccardi, V. Braun, K. Kusume, P. Marsch, M. Maternia, et al., "Scenarios for 5G mobile and wireless communications: the vision of the METIS project," IEEE Communications Magazine, vol. 52, pp. 26-35, 2014.

[3] Pramod Viswanath David Tse. *"Fundamentals of Wireless Communication"*. Cambridge University Press, 2004.

[4] Andrea Goldsmith. "Wireless Communications". Cambridge University Press, 2005.

[5] A.F. Elrefaie, M. Shakouri, "Propagation measurements at 28 GHz for coverage evaluation of local multipoint distribution service", Proceedings of 1997 Wireless Communications Conference, 1997, pp. 12-17.

[6] P.A. Tenerelli, C.W. Bostian, "Measurements of 28 GHz diffraction loss by building corners", Ninth IEEE International Symposium on Personal, Indoor and Mobile Radio Communications (Cat. No.98TH8361), 1998, pp. 1166-1169 vol.3.

[7] C. Briso-Rodriguez, M.A. Vazquez-Castro, J.I. Alonso-Montes, "28 GHz LMDS channel measurements and modeling for parameterized urban environments", 2001 IEEE MTT-S International Microwave Sympsoium Digest (Cat. No.01CH37157), 2001, pp. 2207-2210 vol.3.

[8] S. Geng, J. Kivinen, X. Zhao, P. Vainikainen, "Millimeter-Wave Propagation Channel Characterization for Short-Range Wireless Communications", IEEE Transactions on Vehicular Technology 58(1) (2009) 3-13.

[9] G.R. MacCartney, Z. Junhong, N. Shuai, T.S. Rappaport, "Path loss models

for 5G millimeter wave propagation channels in urban microcells", 2013 IEEE Global Communications Conference (GLOBECOM), 2013, pp. 3948-3953.

[10] Y. Azar, G.N. Wong, K. Wang, R. Mayzus, J.K. Schulz, H. Zhao, F. Gutierrez, D. Hwang, T.S. Rappaport, "28 GHz propagation measurements for outdoor cellular communications using steerable beam antennas in New York city", 2013 IEEE International Conference on Communications (ICC), 2013, pp. 5143-5147.

[11] M. Samimi, K. Wang, Y. Azar, G.N. Wong, R. Mayzus, H. Zhao, J.K. Schulz, S. Sun, F. Gutierrez, T.S. Rappaport, "28 GHz Angle of Arrival and Angle of Departure Analysis for Outdoor Cellular Communications Using Steerable Beam Antennas in New York City", 2013 IEEE 77th Vehicular Technology Conference (VTC Spring), 2013, pp. 1-6.

[12] T.S. Rappaport, F. Gutierrez, E. Ben-Dor, J.N. Murdock, Y. Qiao, J.I. Tamir, "Broadband Millimeter-Wave Propagation Measurements and Models Using Adaptive-Beam Antennas for Outdoor Urban Cellular Communications", IEEE Transactions on Antennas and Propagation 61(4) (2013) 1850-1859.

[13] H. Zhao, R. Mayzus, S. Sun, M. Samimi, J.K. Schulz, Y. Azar, K. Wang, G.N. Wong, F. Gutierrez, T.S. Rappaport, "28 GHz millimeter wave cellular communication measurements for reflection and penetration loss in and around buildings in New York city", 2013 IEEE International Conference on Communications (ICC), 2013, pp. 5163-5167.

[14] G.R. MacCartney, M.K. Samimi, T.S. Rappaport, "Omnidirectional path loss models in New York City at 28 GHz and 73 GHz", 2014 IEEE 25th Annual International Symposium on Personal, Indoor, and Mobile Radio Communication (PIMRC), 2014, pp. 227-231.

[15] G.R. Maccartney, T.S. Rappaport, M.K. Samimi, S. Sun, "Millimeter-Wave Omnidirectional Path Loss Data for Small Cell 5G Channel Modeling", IEEE Access 3 (2015) 1573-1580.

[16] S. Deng, M.K. Samimi, T.S. Rappaport, "28 GHz and 73 GHz millimeter-

wave indoor propagation measurements and path loss models", 2015 IEEE International Conference on Communication Workshop (ICCW), 2015, pp. 1244-1250.

[17] S. Sun, G.R. MacCartney, T.S. Rappaport, "Millimeter-wave distance-dependent large-scale propagation measurements and path loss models for outdoor and indoor 5G systems", 2016 10th European Conference on Antennas and Propagation (EuCAP), 2016, pp. 1-5.

[18] M.K. Samimi, G.R. MacCartney, S. Sun, T.S. Rappaport, "28 GHz Millimeter-Wave Ultrawideband Small-Scale Fading Models in Wireless Channels", 2016 IEEE 83rd Vehicular Technology Conference (VTC Spring), 2016, pp. 1-6.

[19] T. Abbas, F. Qamar, I. Ahmed, K. Dimyati, M.B. Majed, "Propagation channel characterization for 28 and 73 GHz millimeter-wave 5G frequency band", 2017 IEEE 15th Student Conference on Research and Development (SCOReD), 2017, pp. 297-302.

[20] T.S. Rappaport, Y. Xing, G.R. MacCartney, A.F. Molisch, E. Mellios, J. Zhang, "Overview of Millimeter Wave Communications for Fifth-Generation (5G) Wireless Networks—With a Focus on Propagation Models", IEEE Transactions on Antennas and Propagation 65(12) (2017) 6213-6230.

[21] T.S. Rappaport, G.R. MacCartney, S. Sun, H. Yan, S. Deng, "Small-Scale, Local Area, and Transitional Millimeter Wave Propagation for 5G Communications", IEEE Transactions on Antennas and Propagation 65(12) (2017) 6474-6490.

[22] I.A. Hemadeh, K. Satyanarayana, M. El-Hajjar, L. Hanzo, "Millimeter-Wave Communications: Physical Channel Models, Design Considerations, Antenna Constructions, and Link-Budget", IEEE Communications Surveys & Tutorials 20(2) (2018) 870-913.

[23] Rappaport, T.S., et al. (2017). "Overview of Millimeter Wave Communications for Fifth-Generation (5G) Wireless Networks—With a Focus on Propagation Models." IEEE Transactions on Antennas and

Propagation 65(12): 6213-6230.

[24] Smirnov, N. I., et al. (2017). Increase in the efficiency of the coverage area in the cellular communication systems. 2017 Systems of Signal Synchronization, Generating and Processing in Telecommunications (SINKHROINFO).

[25] https://www.anokiwave.com/products/index.html

[26] Sajal Kumar Das ,First published: 30 September https://doi.org/10.1002/9781119107422.ch1

[27] http://www.radartutorial.eu/09.receivers/rx51.en.html

[28] 5Gseminar_Huawei_Lombardi

[29] Islam, M. N., et al. (2017). Integrated Access Backhaul in Millimeter Wave Networks. 2017 IEEE Wireless Communications and Networking Conference (WCNC).

[30] 3GPP, "Study on Integrated Access and Backhaul for NR," AT&T, Qualcomm, Samsung - Tdoc RP-171880, 2017.

[31] Polese, M., et al. (2018). End-to-End Simulation of Integrated Access and Backhaul at mmWaves. 2018 IEEE 23rd International Workshop on Computer Aided Modeling and Design of Communication Links and Networks (CAMAD).

[32] G. R. MacCartney Jr. and T. S. Rappaport, "73 GHz millimeter wave propagation measurements for outdoor urban mobile and backhaul communications in New York City," in Proc. IEEE ICC, Jun. 2014, pp. 4862–4867.

[33] T. S. Rappaport et al., "Millimeter wave mobile communications for 5G cellular: It will work!" IEEE Access, vol. 1, pp. 335–349, May 2013.

[34] Samimi, M. K., et al. (2015). "Probabilistic Omnidirectional Path Loss Models for Millimeter-Wave Outdoor Communications." IEEE Wireless Communications Letters 4(4): 357-360.